INTERNAL DUAL-BAND PATCH ANTENNA FOR MOBILE PHONES

Jani Ollikainen, Outi Kivekäs, Anssi Toropainen, and Pertti Vainikainen

Helsinki University of Technology,
Institute of Radio Communications,
Radio Laboratory,
P.O. Box 3000, FIN-02015 HUT, Finland
Email: jol@radio.hut.fi

INTRODUCTION

Development of small antennas for mobile phones has received a lot of attention during the last few years due to size reduction of the handsets, requirements to keep the amount of RF power absorbed by the user below standardized levels regardless of the handset size, and introduction of multimode phones. Single-band and dual-band phones in which the external whip or helix antenna has been replaced by an internal shorted patch antenna (or PIFA) are already in the market. It may be assumed that in the future there will also be a need for internal antennas which operate in several communication systems. In this paper, a multiresonant dual-band internal handset antenna is introduced. The antenna is based on the dual-resonant antenna structure reported in [1]. To our knowledge, this is the first internal handset antenna which covers the E-GSM900 (880 MHz - 960 MHz), GSM1800 (1710 MHz - 1880 MHz), DECT (1880 MHz - 1900 MHz), PCS1900 (1850 MHz - 1990 MHz), and UMTS (1900 MHz - 2170 MHz) frequencies with a return loss $L_{retn} \geq 6$ dB and high radiation efficiency. Previously shorted patch antennas (or PIFAs) with more than one band of operation have been reported e.g. in [2-4]. The dual-band PIFA was introduced in [2]. The idea was extended to multiband PIFAs in [3]. A compact dual-band PIFA with two capacitive feeds was reported in [4].

ANTENNA DESIGN

The studied antenna consists of three shorted patches, one for the lower band and two for the upper band. The lower band patch (parts a-c in Fig. 1) and one of the upper band patches (part d) have been joined together to form a dual-band element having only one short circuit and one feed. This dual-band element has been folded into a meander line -like shape to better fit it into the geometry of a mobile phone. The third shorted patch (part e) is positioned next to the upper band section of the dual-band element to obtain a doubly tuned resonance and a wider impedance bandwidth at the upper band. The dielectric between the patches and the ground plane is air (relative permittivity $\varepsilon_r' = 1$). The antenna is fed by a probe which is connected to the upper band patch of the dual-band element. The total size of the antenna element is 40 mm × 30.4 mm × 7.2 mm (*width* × *length* × *thickness*). It is positioned on top of a ground plane having dimensions 40 mm × 110 mm × 0.3 mm (*width* × *length* × *thickness*). The length and width of the ground plane were selected to be approximately equal to those of the printed circuit board of a typical mobile phone. The antenna structure was designed and theoretically studied using IE3D which is a moment method-based 3D electromagnetic simulation program by Zeland Software.

A prototype antenna was constructed by photoetching the patches, short circuits and the capacitive load from 0.2 mm-thick sheet of tin bronze (contains 96 % copper and 4 % tin, conductivity $\sigma = 1.1 \cdot 10^7$ S/m). The ground plane was made out of 0.3 mm-thick sheet of the same material. The patches are supported above the ground plane by the short circuits, the feed probe, and a 40 mm × 10 mm × 7 mm piece of Styrofoam.

Acknowledgements - The postgraduate studies of the first two authors have been financially supported by the Academy of Finland, Graduate School in Electronics, Telecommunications and Automation (GETA), Jenny and Antti Wihuri Foundation, Nokia Foundation, and Tekniikan Edistämissäätiö. The radiation patterns of the constructed prototype antenna were measured in the anechoic chamber of LK-Products, Finland.

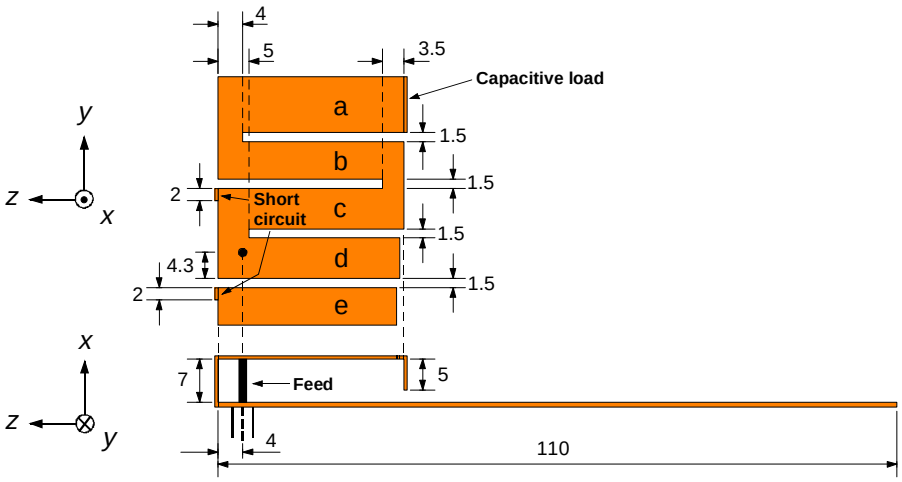

Part	Length (mm)	Width (mm)
a	30	9
b	30	6
c	30	6.5
d	29	6.5
e	28.8	6

Fig. 1. Studied antenna configuration. All dimensions are in millimeters.

RESULTS

The frequency responses of the measured and simulated reflection coefficients are shown in Fig. 2. A good agreement between the simulated and measured results can be observed. The measured impedance bandwidth ($L_{retn} \geq 6$ dB) of the lowest band is 12.4 % (115 MHz) at the center frequency f_c = 926 MHz. For the dual-resonant upper band, the measured bandwidth ($L_{retn} \geq 6$ dB) is 27.7 % (535 MHz) at f_c = 1934 MHz. Above the desired bands, there is also a third band with the bandwidth of 3.6 % (89 MHz) at f_c = 2515 MHz. The third band is assumed to be caused by the $3\lambda/4$-resonance of the lower band section of the meandered antenna element. This resonance has been tuned down from 2700 MHz by the presence of the upper band section of the meandered dual-band element (part d in Fig.1). According to simulations, the impedance bandwidth of the antenna depends on the length of the ground plane. However, in this design the ground plane length is not optimized with respect to the bandwidth.

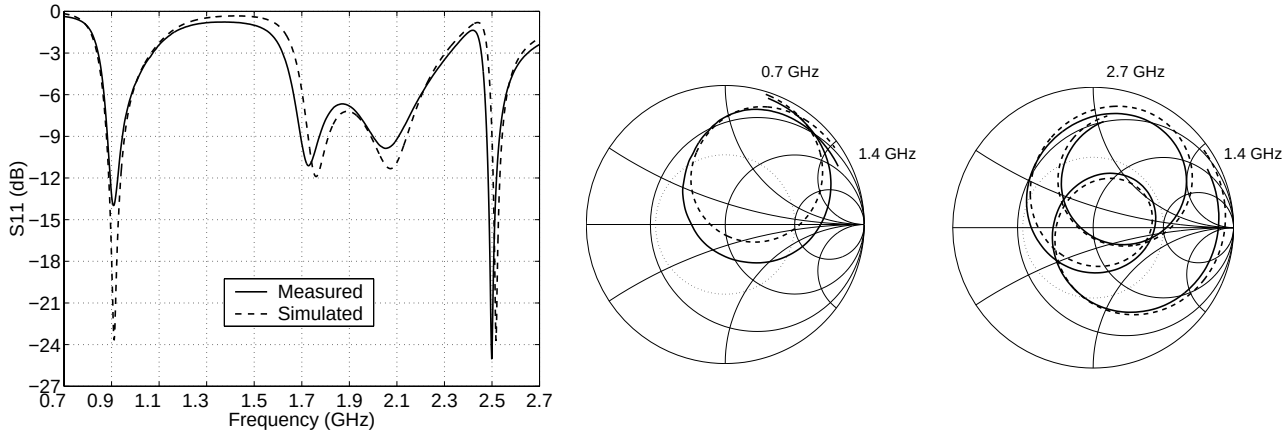

Fig. 2. Measured (solid line) and simulated (dashed line) reflection coefficient as a function of frequency. Dotted circles on the Smith charts represent L_{retn} = 6 dB.

The measured and simulated cuts of the radiation patterns of the studied antenna are shown in Fig. 3. The presented cuts have been obtained in free space. At 920 MHz, the radiation pattern is almost omnidirectional and resembles that of a half-wave dipole. At 1710 MHz, the pattern becomes more complex and somewhat more directive. The directivity increases with frequency. At the same time the pattern maximum tilts towards the negative *z*-axis. In addition, it can be seen in Fig. 3 that the polarization of the antenna at the lower band is different from the polarization at the upper band.

Fig. 4. shows the simulated radiation efficiency (IE3D) of the antenna in free space. The conductivity used in the calculations was $\sigma = 1.1 \cdot 10^7$ S/m. The efficiency stays above 95 % over the two desired bands of operation.

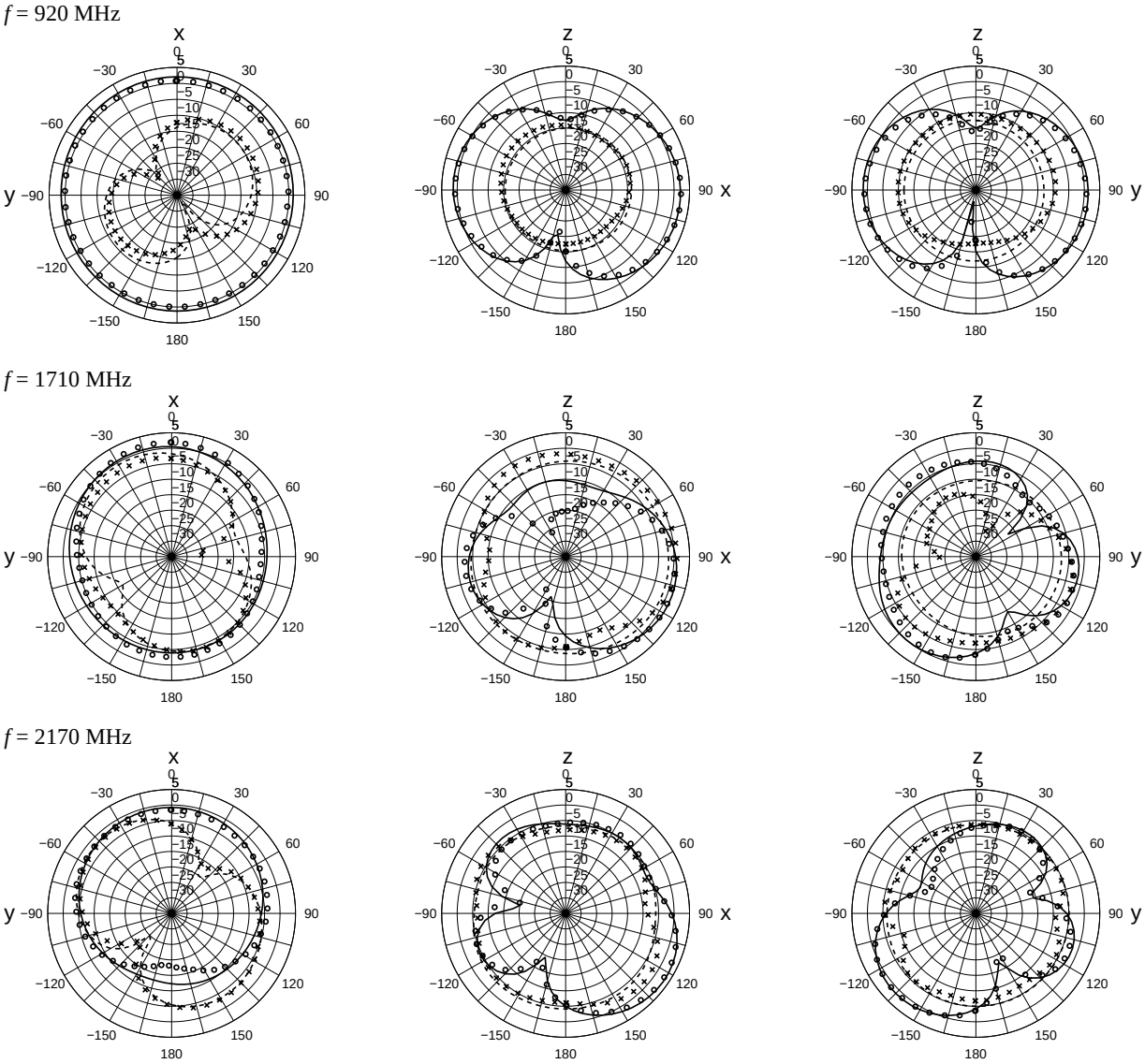

Fig. 3. Measured (o o o E_θ , x x x E_φ) and simulated (—— E_θ , – – – E_φ) cuts of the radiation patterns at 920 MHz, 1710 MHz, and 2170 MHz. Antenna orientation is given in Fig. 1. Results include the effect of mismatch loss. Radial unit is dBi.

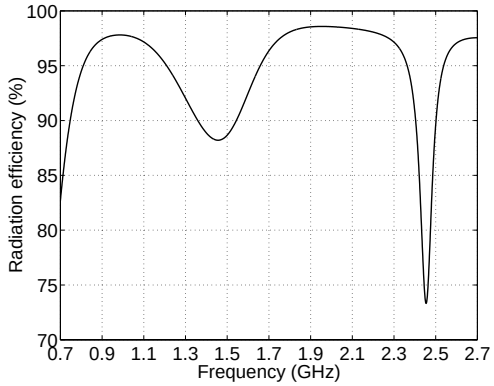

Fig. 4. Simulated (IE3D) radiation efficiency in free space as a function of frequency for the studied antenna. Conductivity of metal parts $\sigma = 1.1 \cdot 10^7$ S/m.

The specific absorption rate (*SAR*) characteristics of the studied antenna were evaluated by simulations which were performed using a commercial FDTD program (XFDTD, version 5.0 Bio-Pro by Remcom, Inc.). An FDTD mesh of a male head and shoulders with the voxel resolution of 2.5 mm was used. This was based on the standard human head and shoulders mesh (3 mm voxel) obtained from Remcom. The values of the tissue parameters (ε_r', σ_{eff}) were interpolated from the values given in [5]. The tissue density values were those provided with the original mesh. The phone model (antenna and thin ground plane) was placed beside the head model according to the intended use position specified by CENELEC [6]. This was obtained by rotating the head model forward by 74° and to the right by 10° while keeping the phone model vertical in the mesh. The distance of 11.9 mm (5 cells) was left between the head and phone model. The *SAR*s were calculated at 915 MHz, 1730 MHz, and 2100 MHz using a steady-state sinusoidal excitation. Due to the limitations of the 2.5 mm grid, the dimensions of the antenna, and thus also its resonant frequencies, were slightly different from those of the measured antenna. The frequencies used in *SAR* simulations were adjusted accordingly. The simulation space enclosing the head and the handset consisted of 207 × 187 × 206 cells. The simulations were run for 4000 timesteps to ensure converged results.

The results of the *SAR* simulations are listed in Table 1. The maximum 10 g average *SAR* value was located near the center of the ground plane at 915 MHz. At 1730 MHz, the maximum was found near the short circuit of the parasitic resonator (part e in Fig. 1), and at 2100 MHz near the short circuit of the meandered patch. The results indicate that the *SAR*s are below the basic restrictions set by CENELEC. When studying the *SAR* values given in Table 1, it must be noted that the specified mean (rms) output powers for handsets in GSM900, GSM1800, DECT, and UMTS systems are 250 mW, 125 mW, 10 mW, and 250 mW, respectively. The radiation efficiencies when the phone model is beside the head are also listed in Table 1. The radiation efficiencies at 1730 MHz and 2100 MHz are more than twice as high as the efficiency at 915 MHz. This is partly explained by more directive radiation patterns at 1730 MHz and 2100 MHz.

Table 1. Simulated maximum 10 g average *SAR* values in the head, and simulated radiation efficiencies (XFDTD) with prototype beside the head. *SAR* results are normalized to 1 W of CW input power.

f (MHz)	915	1730	2100
Max 10 g average *SAR* (W/kg)	4.6	1.8	1.8
Radiation efficiency (%)	29	72	75

CONCLUSIONS

A multiresonant internal dual-band shorted patch antenna for mobile phones has been studied. Both simulated and measured results have been presented. The studied antenna has two bands of operation, the lower one ranges from 868 MHz to 983 MHz (12.4 %) and the upper one from 1666 MHz to 2201 MHz (27.7 %). The radiation patterns are suitable for internal handset antenna application. According to simulated results with FDTD, the *SAR* values caused by the antenna are below the limits set by CENELEC.

REFERENCES

[1] J. Ollikainen and P. Vainikainen, "Radiation and bandwidth characteristics of two planar multistrip antennas for mobile communication systems," *Proc. IEEE 48th Vehicular Technology Conference*, Vol. II, Ottawa, Ontario, Canada, May 18-21, 1998, pp. 1186-1190.

[2] Z. D. Liu, P. S. Hall, and D. Wake, "Dual-frequency planar inverted-F antenna", *IEEE Transactions on Antennas and Propagation*, Vol. 45, No. 10, October 1997, pp. 1451-1458.

[3] P. Song, P.S. Hall, H. Ghafouri-Shiraz, and D. Wake, "Triple-band planar inverted-F antenna", *IEEE Antennas and Propagation International Symposium Digest*, Vol. 2, Orlando, Florida, July 11-16, 1999, pp. 908-911.

[4] C. R. Rowell and R. D. Murch, "A compact PIFA suitable for dual-frequency 900/1800-MHz operation", *IEEE Transactions on Antennas and Propagation*, Vol. 46. No. 4, April 1998, pp. 596-598.

[5] *User's Manual for XFDTD the Finite Difference Time Domain Graphical User Interface for Electromagnetic Calculations*, Version 5.04, Remcom, Inc., February 1999, 128 p.

[6] European specification (ES 59005), *Considerations for the Evaluation of Human Exposure to Electromagnetic Fields (EMFs) from Mobile Telecommunication Equipment (MTE) in the Frequency Range 30 MHz - 6 GHz*, Brussels, Belgium, CENELEC, October 1998, 81 p.

射 频 和 天 线 设 计 培 训 课 程 推 荐

易迪拓培训(www.edatop.com)由数名来自于研发第一线的资深工程师发起成立，致力并专注于微波、射频、天线设计研发人才的培养；我们于 2006 年整合合并微波 EDA 网(www.mweda.com)，现已发展成为国内最大的微波射频和天线设计人才培养基地，成功推出多套微波射频以及天线设计经典培训课程和 ADS、HFSS 等专业软件使用培训课程，广受客户好评；并先后与人民邮电出版社、电子工业出版社合作出版了多本专业图书，帮助数万名工程师提升了专业技术能力。客户遍布中兴通讯、研通高频、埃威航电、国人通信等多家国内知名公司，以及台湾工业技术研究院、永业科技、全一电子等多家台湾地区企业。

易迪拓培训课程列表：http://www.edatop.com/peixun/rfe/129.html

射频工程师养成培训课程套装

该套装精选了射频专业基础培训课程、射频仿真设计培训课程和射频电路测量培训课程三个类别共 30 门视频培训课程和 3 本图书教材；旨在引领学员全面学习一个射频工程师需要熟悉、理解和掌握的专业知识和研发设计能力。通过套装的学习，能够让学员完全达到和胜任一个合格的射频工程师的要求…

课程网址：http://www.edatop.com/peixun/rfe/110.html

ADS 学习培训课程套装

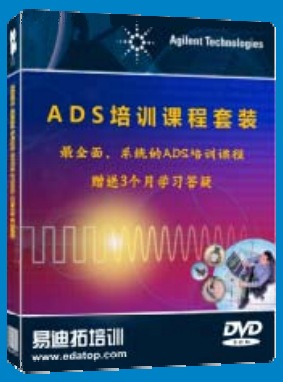

该套装是迄今国内最全面、最权威的 ADS 培训教程，共包含 10 门 ADS 学习培训课程。课程是由具有多年 ADS 使用经验的微波射频与通信系统设计领域资深专家讲解，并多结合设计实例，由浅入深、详细而又全面地讲解了 ADS 在微波射频电路设计、通信系统设计和电磁仿真设计方面的内容。能让您在最短的时间内学会使用 ADS，迅速提升个人技术能力，把 ADS 真正应用到实际研发工作中去，成为 ADS 设计专家...

课程网址： http://www.edatop.com/peixun/ads/13.html

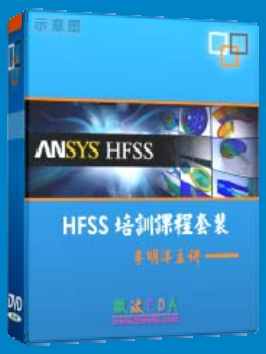

HFSS 学习培训课程套装

该套课程套装包含了本站全部 HFSS 培训课程，是迄今国内最全面、最专业的 HFSS 培训教程套装，可以帮助您从零开始，全面深入学习 HFSS 的各项功能和在多个方面的工程应用。购买套装，更可超值赠送 3 个月免费学习答疑，随时解答您学习过程中遇到的棘手问题，让您的 HFSS 学习更加轻松顺畅…

课程网址：http://www.edatop.com/peixun/hfss/11.html

CST 学习培训课程套装

该培训套装由易迪拓培训联合微波 EDA 网共同推出，是最全面、系统、专业的 CST 微波工作室培训课程套装，所有课程都由经验丰富的专家授课，视频教学，可以帮助您从零开始，全面系统地学习 CST 微波工作的各项功能及其在微波射频、天线设计等领域的设计应用。且购买该套装，还可超值赠送 3 个月免费学习答疑…

课程网址：http://www.edatop.com/peixun/cst/24.html

HFSS 天线设计培训课程套装

套装包含 6 门视频课程和 1 本图书，课程从基础讲起，内容由浅入深，理论介绍和实际操作讲解相结合，全面系统的讲解了 HFSS 天线设计的全过程。是国内最全面、最专业的 HFSS 天线设计课程，可以帮助您快速学习掌握如何使用 HFSS 设计天线，让天线设计不再难…

课程网址：http://www.edatop.com/peixun/hfss/122.html

13.56MHz NFC/RFID 线圈天线设计培训课程套装

套装包含 4 门视频培训课程，培训将 13.56MHz 线圈天线设计原理和仿真设计实践相结合，全面系统地讲解了 13.56MHz 线圈天线的工作原理、设计方法、设计考量以及使用 HFSS 和 CST 仿真分析线圈天线的具体操作，同时还介绍了 13.56MHz 线圈天线匹配电路的设计和调试。通过该套课程的学习，可以帮助您快速学习掌握 13.56MHz 线圈天线及其匹配电路的原理、设计和调试…

详情浏览：http://www.edatop.com/peixun/antenna/116.html

我们的课程优势：

※ 成立于 2004 年，10 多年丰富的行业经验，

※ 一直致力并专注于微波射频和天线设计工程师的培养，更了解该行业对人才的要求

※ 经验丰富的一线资深工程师讲授，结合实际工程案例，直观、实用、易学

联系我们：

※ 易迪拓培训官网：http://www.edatop.com

※ 微波 EDA 网：http://www.mweda.com

※ 官方淘宝店：http://shop36920890.taobao.com